



# The ECHO code for astrophysical plasmas: from classic to general relativistic MHD

<http://www.astro.unifi.it/echo/>

L. Del Zanna, S. Landi – Dipartimento di Astronomia e Scienza dello Spazio, Università di Firenze  
P. Londrillo – Osservatorio Astronomico di Bologna, INAF



ASAP – ARCRETI SPACE & ASTROPHYSICAL PLASMAS

## Introduction

ECHO (Eulerian Conservative High Order) is a general-purpose modular code for hyperbolic equations. In particular for classical MHD [1], special relativistic MHD [2], general relativistic MHD [3], and their hydrodynamics counterparts. It is designed to combine *shock-capturing properties* for discontinuities together with *accuracy* for small-scale wave propagation and turbulence.

Like MHD, GRMHD is a single-fluid (ideal) closure for plasmas. It is the relativistic extension of MHD, accounting in addition for: strong gravity, fast speeds, extremely hot plasmas, strong magnetic fields, electric force and displacement current.

Examples in High-Energy Astrophysics involving compact objects and GRMHD flows are:

- Launching and propagation of AGN jets
- Non-spherical accretion onto Black Holes
- Jets from collapsars as GRB progenitors
- Merging of neutron stars and collapse to a Black Hole

## The 3+1 GRMHD conservative equations

The covariant GRMHD equations are first split in time and space according to the so-called 3+1 formalism:

$$ds^2 = -\alpha^2 dt^2 + \gamma_{ij}(dx^i + \beta^i dt)(dx^j + \beta^j dt)$$

The following set of conservative equations may be derived for the variables  $D, S, U, B$  [3]:

$$\partial_t(\gamma^{1/2} D) + \partial_i[\gamma^{1/2}(\alpha v^i - \beta^i)D] = 0$$

$$\partial_t(\gamma^{1/2} S) + \partial_i[\gamma^{1/2}(\alpha W^i - \beta^i S)] = \gamma^{1/2}(\alpha W^a \partial_a \gamma_{ij} / 2 + S \partial_i \beta^j - U \partial_i \alpha)$$

$$\partial_t(\gamma^{1/2} U) + \partial_i[\gamma^{1/2}(\alpha S^i - \beta^i U)] = \gamma^{1/2}(\alpha K_j W^j - S^i \partial_i \alpha)$$

$$\partial_t(\gamma^{1/2} B^i) + \partial_j[\gamma^{1/2}(\alpha v^j - \beta^j)B^i - \gamma^{1/2}(\alpha v^i - \beta^i)B^j] = 0; \quad \partial_i(\gamma^{1/2} B^i) = 0$$

The lapse function  $\alpha$ , shift vector  $\beta$ , metric 3-tensor  $\gamma$  and the extrinsic curvature  $K$  contain the gravitational effects and may be even time-dependent (given or evolved through Einstein's equations). Only familiar spatial 3-D vectors and tensors are involved:

$$D = \rho \Gamma; \quad \vec{S} = \rho h \Gamma^{-1} \vec{v} + \vec{E} \times \vec{B}; \quad U = \rho h \Gamma^{-2} - p + (E^2 + B^2)/2$$

$$\vec{W} = \rho h \Gamma^{-2} \vec{v} + p \vec{\gamma} - \vec{E} \vec{E} - \vec{B} \vec{B} + (E^2 + B^2)/2 \vec{\gamma}; \quad \vec{E} = -\vec{v} \times \vec{B}$$

Here  $\rho$  is the plasma proper density,  $\vec{v}$  is the 3-velocity,  $\vec{E}$  and  $\vec{B}$  the electromagnetic fields,  $p$  the thermal pressure,  $\Gamma$  the bulk Lorentz factor, and  $h$  the specific enthalpy (including rest mass energy density), that for a perfect gas with  $\gamma$ -law EoS is  $h = 1 + \varepsilon + p/\rho = 1 + 4p/\rho$  ( $\gamma = 4/3$ )

The special relativistic case is found when  $\alpha \rightarrow 1$ ,  $\beta \rightarrow 0$ ,  $K \rightarrow 0$ . Classical MHD is retrieved when also  $v \ll c$  ( $\Gamma \rightarrow 1$ ,  $E \ll B$ ), and  $p \ll \rho$  ( $h \rightarrow 1$ ). Any curvilinear set of spatial coordinates is allowed by choosing the appropriate 3-tensor  $\gamma$ .

Standard numerical techniques for solving hyperbolic set of equations may be applied (Godunov-type methods).

## The ECHO scheme

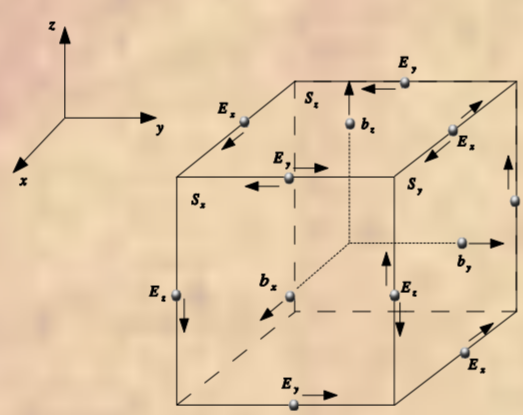
ECHO is designed with a modular structure (GRMHD, GRMHD, RMHD, MHD and their hydrodynamical counterparts), it is written in Fortran 90, and employs MPI directives for parallelization. The main numerical features are briefly reported below.

• The set of conservation laws is discretized in space (finite differences) according to the Upwind Constrained Transport (UCT) strategies [4]. The fluid and the magnetic field equations become:

$$\frac{d}{dt}[u]_c + \sum_i \frac{1}{h_i} ([f]_{i,c} - [f]_{i,c}^*) = [s]_c$$

$$\frac{d}{dt}[b]_{s,c} + \sum_{i,j,k} [ijk]_{s,c} \frac{1}{h_i} ([\hat{e}]_{i,c} - [\hat{e}]_{i,c}^*) = 0; \quad \sum_i \frac{1}{h_i} ([\hat{b}]_{i,c} - [\hat{b}]_{i,c}^*) = 0$$

$$b^i = \gamma^{1/2} B^i; \quad e_i = -[ijk] \tilde{v}^j b^k; \quad \tilde{v}^i = \alpha v^i - \beta^i$$



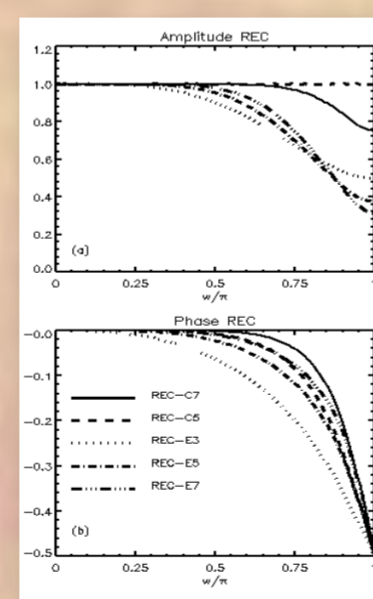
UCT discretization of variables in a single grid cell.

Staggered locations for magnetic and electric field components (Stokes rather than Gauss): point values at cell centers (variables  $u$ ), at cell faces ( $b$  and  $f$  fluxes), at edges ( $e$ ).

The *hat* indicates high-order differencing. The UCT method preserves the solenoidal condition even in the presence of shocks (to machine accuracy for second order schemes).

• System-independent, component-wise, 1-D high-order procedures (REC, DER, INT):

1. **REC**onstruction (upwind L-R primitive variables)
  - ✓ PLM (with a selection of different limiters), PPM
  - ✓ WENO-3, WENO-5, WENO-7, CENO-3
  - ✓ Fixed explicit stencils (3,5,7<sup>th</sup> order) + Monotonicity Preserving for upwinding
  - ✓ Compact implicit routines with spectral-like resolution + MP
2. **DER**ivation (centered, needed for *hat* fluxes)
  - ✓ Fixed explicit or compact (4,6,8<sup>th</sup> order)
3. **INT**erpolation (centered, needed to derive  $B$  from  $b$ )
  - ✓ Fixed explicit or compact (4,6,8<sup>th</sup> order)



Spectral behavior of some explicit and compact high-order REC routines (without limiter) as a function of the normalized wavevector. Optimal spectral resolution would be 1 for the amplitude and 0 for the phase.

• System-independent two-wave Riemann solver (HLL), only the fastest characteristic speeds are needed. The UCT method requires a *four-state* electric field at cell edges.

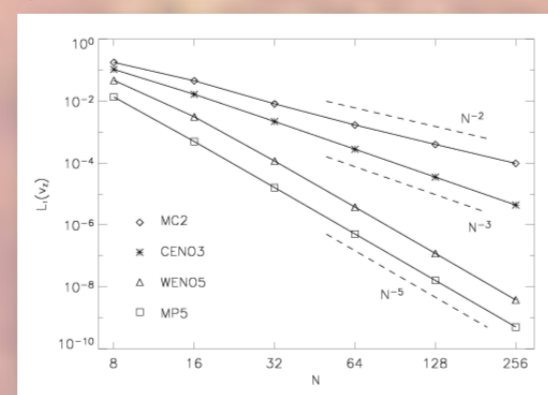
• Runge-Kutta time-stepping (2,3,4<sup>th</sup> order).

## Numerical tests: high-order accuracy

Alfvén wave propagation along the diagonal of a square domain provides an excellent test to check the high-order procedures of a numerical scheme. An exact solution for a large-amplitude circularly-polarized wave has been found also for special relativistic MHD [3]. For a scheme of accuracy  $r$  in both space and time, the errors on any variable  $u$  after a period  $T$  should scale like

$$L_2(u) = \sum_i |u(x_i, y_i, T) - u(x_i, y_i, 0)| / N^i \propto N^{-r}$$

as a function of the number  $N$  of grid points along one direction. The figure shows that in ECHO this is indeed the case. Here only the results for a selection of explicit REC routines are shown.

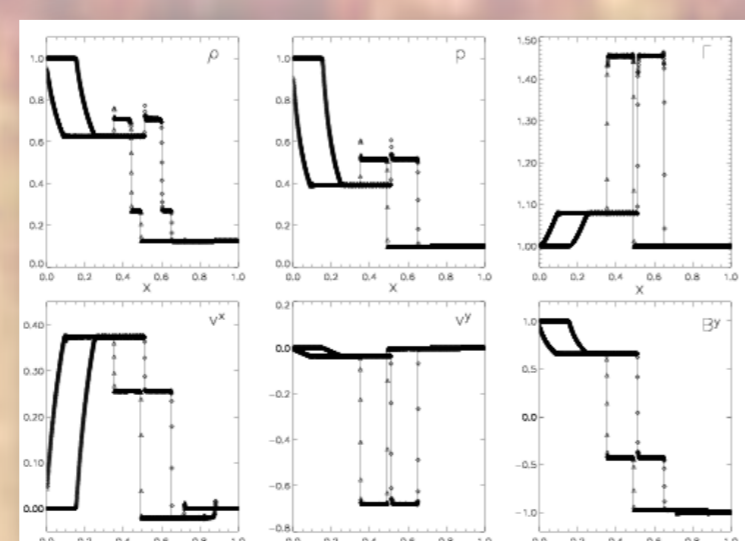


RMHD CP Alfvén wave test in a Cartesian 2-D domain.

## Numerical tests: shock-capturing properties

The shock-capturing properties of ECHO are tested by comparing the numerical solution for a 1-D Riemann problem (diamonds in figure) with the corresponding analytical solution. The test chosen is the special relativistic version of the so-called Brio-Wu MHD problem, in which a compound wave is present in the numerical solution. Here an explicit fifth order REC + MP has been employed but the overall accuracy is kept to second order.  $N=1600$  grid points have been used. In order to test also general relativistic effects, two different cases are shown: one with  $\alpha > 1$  and another with  $\beta > 0$ , to be compared with the exact solution shifted in time or space, respectively:

$$\alpha > 1 \Rightarrow t = t_{max}/\alpha, \quad \beta > 0 \Rightarrow x = x - \beta t_{max}$$



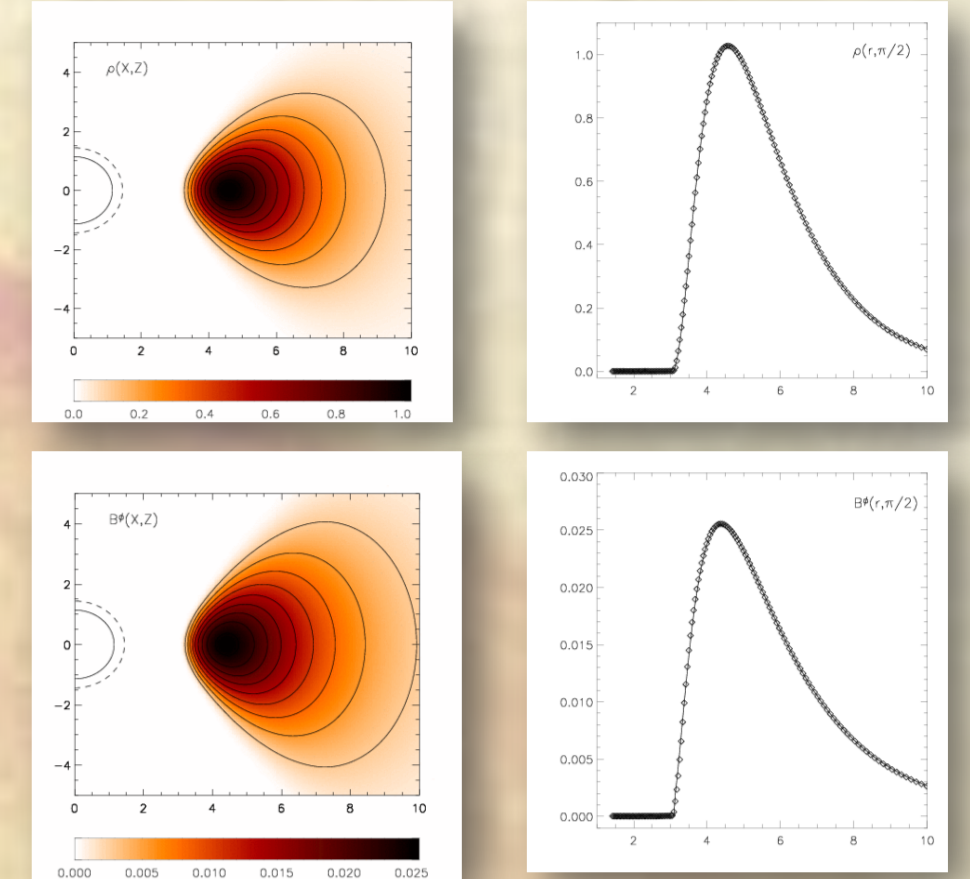
RMHD Riemann problem (relativistic Brio-Wu test) in a 1-D Cartesian domain.

## Numerical tests: magnetized thick torus around a Kerr black hole

The most complex problem with an analytical exact solution that can be used as a test for a GRMHD code is that of a magnetized thick torus in stationary equilibrium around a Kerr black hole. For a constant specific angular momentum disk and assuming polytropic laws for thermal and magnetic pressures (here a purely toroidal field is considered), an axisymmetric solution is derived from a potential  $W(r, \theta)$  as:

$$W - W_e + \frac{\gamma}{\gamma-1} \frac{p+B^2/2}{\rho h} = 0; \quad W = \ln(-u) = \frac{1}{2} \ln \left( \frac{g_{\theta\theta}^2 - g_{\theta\phi} g_{\phi\theta}}{g_{\theta\theta} + 2g_{\theta\phi} + g_{\phi\theta}^2} \right)$$

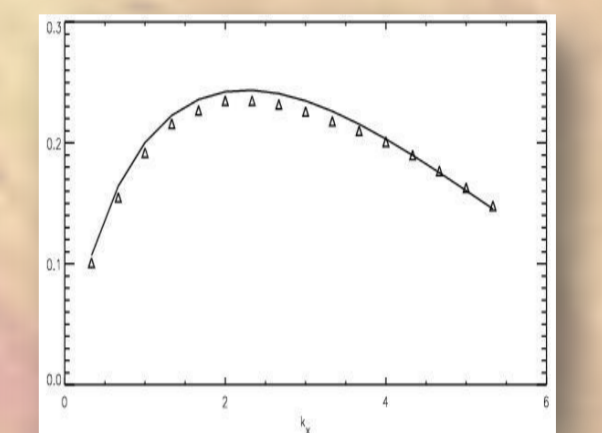
In the numerical test we use  $a=0.99$  (a nearly maximally rotating hole),  $\gamma=4/3$ , 200 grid points in the radial direction and 100 along  $\theta$ . Boyer-Lindquist coordinates are employed with a stretched radial grid, extending from  $r=1.4$  (just outside the event horizon) to  $r=50$ . In the figure we show density and magnetic field distributions (left panels), together with 1-D radial cuts on the equatorial plane, compared with the initial solutions.



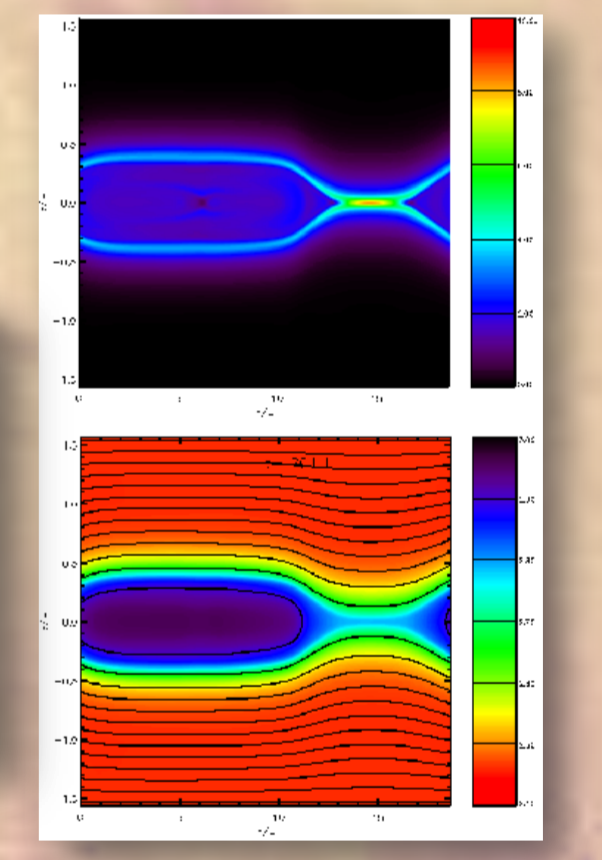
Numerical solution after  $t=200$  (about three orbital periods) compared with the initial solution.

## Applications: compressible MHD tearing mode and turbulence

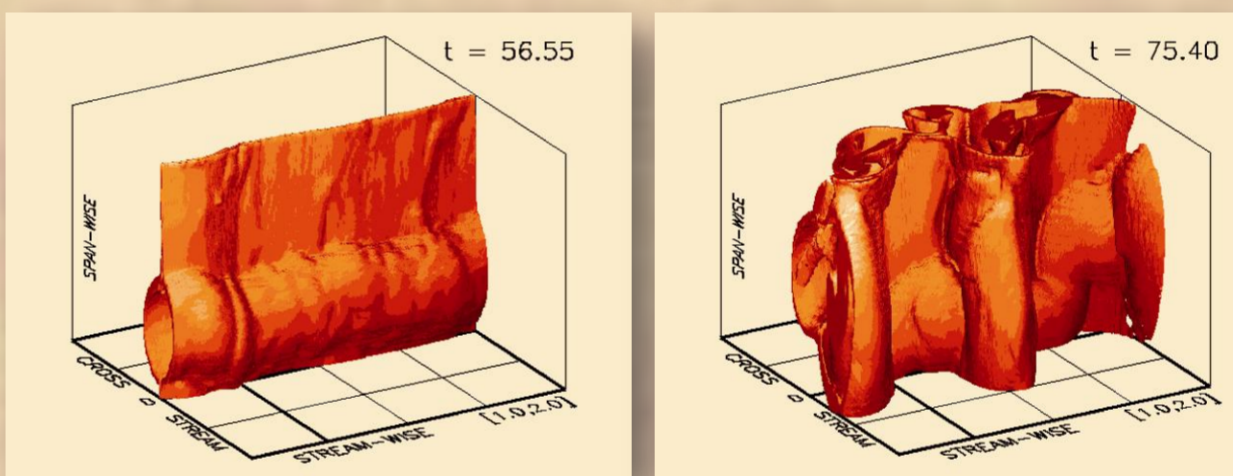
In many astrophysical environments, like the Heliosphere, magnetic diffusivity is at the base of several phenomena (e.g. solar flares). The MHD module of ECHO has been recently upgraded with the inclusion of explicit viscous and resistive terms, to allow studies of non-ideal instabilities in plasmas [5]. In such processes small scales energy transfer is an important ingredient and hence high-orders and good spectral resolution numerical schemes are essential. As an example of application, we report here a numerical experiment of a resistive instability developing in a current sheet (the so-called tearing instability). We have first tested various numerical schemes and we have verified that only when higher order schemes (implicit 5<sup>th</sup> and 7<sup>th</sup> order) are employed resistivity can be appreciated against numerical diffusivity. Using a 7<sup>th</sup> order implicit numerical scheme we have then verified the ability of the numerical code in reproducing correctly the growth rate of the most unstable modes as predicted by the linear theory. The 2-D evolution of the tearing instability is then followed by the coalescence process: the final stage is characterized by the presence of a single magnetic island and a current sheet connecting the two sides (the system is considered to be periodic along the current sheet). The non-linear evolution of such systems can be very different in a fully 3-D system: depending on the initial magnetic configuration which forms the tearing unstable current sheet, the coalescence process can be overwhelmed by a secondary ideal instability in the third direction: the magnetic island is kinked and a more turbulent state is recovered at the later stage of the system evolution.



Comparison between the dispersion relation predicted by the linear theory of the tearing instability (solid line) and that obtained by 2-D simulations using ECHO. The numerical scheme here adopted is the implicit 7<sup>th</sup> order.



Non linear evolution of the 2-D tearing instability. Top: current density intensity. Bottom: Magnetic field lines and pressure (color scale).



3-D plasma structure in the non linear phase of the resistive instability of a current sheet. The current sheet is initially located in the middle of the cross-stream direction and parallel to the stream-wise direction. The equilibrium is characterized by a force-free configuration with the magnetic field far from the current-sheet directed along the span-wise direction. The coalescence process is observed (formation of a magnetic island) in the first part of the non linear regime but it is then followed by a secondary (ideal) instability which drives the system towards a more turbulent state.

## Applications: relativistic MHD model for Pulsar Wind Nebulae

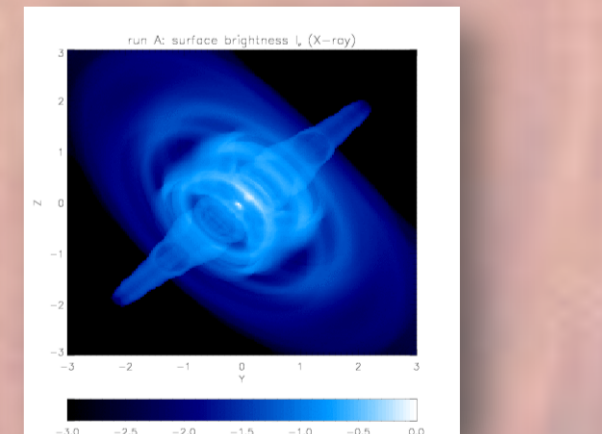
Pulsar Wind Nebulae (PWNe) arise from the confinement of the ultra-relativistic wind produced by a young pulsar by the external expanding supernova remnant. A relativistically hot bubble of plasma and enhanced magnetic fields is produced and non-thermal emission (synchrotron and Inverse Compton scattering) is emitted at all wavelengths. Recently the X-ray Chandra spacecraft has shown an unexpected jet-torus structure of the inner regions of the Crab and other PWNe and mildly relativistic motions are also measured.

Relativistic axisymmetric MHD simulations performed by ECHO [6] are able to reproduce this scenario if the wind energy distribution is anisotropic and stronger near the equatorial plane. There the outflow is further collimated and, if the wind magnetization is high enough, hoop stresses are able to deviate part of it toward the polar axis (the jets).

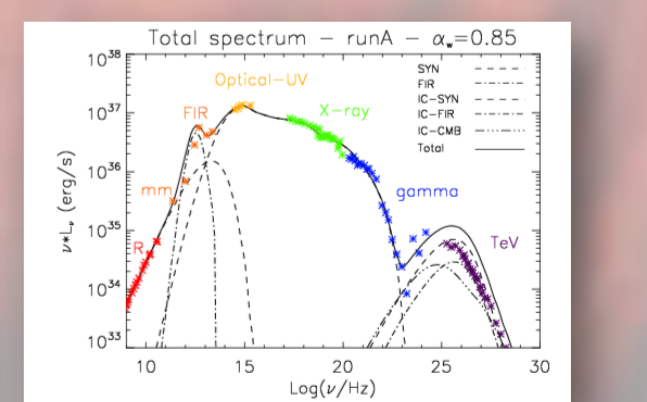
A powerful diagnostic tool has been obtained by adding to the RMHD module of ECHO of an extra equation (in conservative form) for the evolution of the maximum energy attainable by the ultra-relativistic particles produced at the termination shock and then carried away along streamlines:

$$\frac{\partial}{\partial t} (\Gamma \rho^{2\alpha} \varepsilon_{\max}) + \nabla \cdot (\Gamma \rho^{2\alpha} \varepsilon_{\max} \vec{v}) = \frac{4e^+}{9m^+ c^3} \rho^{2\alpha} (B^i)^2 \varepsilon_{\max}^2$$

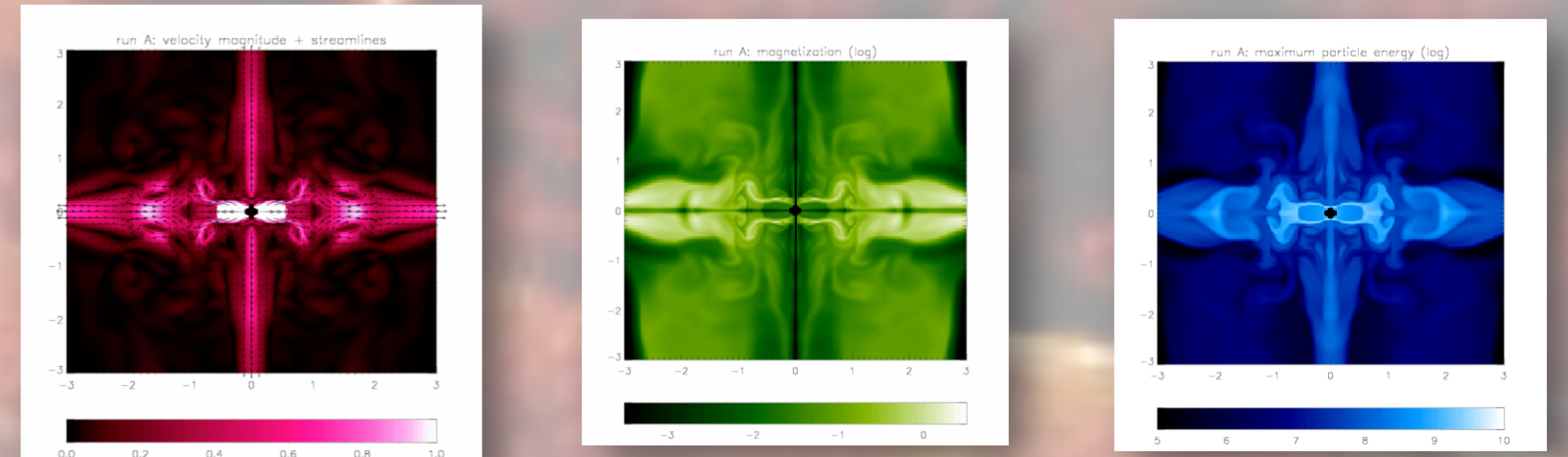
The knowledge of this cut-off energy allows to work out the local synchrotron and Inverse Compton emissivity, so synthetic maps can be produced and matched with observations, to infer physical parameters (e.g. magnetization and wind anisotropy) otherwise unknown [7,8].



The simulated synchrotron X-ray image of the Crab Nebula.



The Crab Nebula spectrum from radio to gamma-ray: model and observations.



Various quantities from the axisymmetric RMHD model of PWNe: from left to right the flow speed in units of  $c$ , the magnetization and the maximum particles energy.

## References

- [1] Londrillo, P., and Del Zanna, L., 2000. High-order upwind schemes for multidimensional magnetohydrodynamics. *ApJ*, 530, 508
- [2] Del Zanna, L., Bucciantini, N., and Londrillo, P., 2003. An efficient shock-capturing central-type scheme for multidimensional relativistic flows. *II magnetohydrodynamics*, *A&A*, 400, 397
- [3] Del Zanna, L., Zanotti, O., Bucciantini, N., and Londrillo, P., 2007. ECHO: a Eulerian conservative high-order scheme for general relativistic magnetohydrodynamics and magnetodynamics. *A&A*, 473, 11
- [4] Londrillo, P., and Del Zanna, L., 2004. On the divergence-free condition in Godunov-type schemes for ideal magnetohydrodynamics: the upwind constrained transport method. *JCP*, 195, 17
- [5] Landi, S., Londrillo, P., Velli, M., and Bettarini, L., 2008. Three-dimensional simulations of compressible tearing instability. *Phys. Plasmas*, 15, 12302
- [6] Del Zanna, L., Amato, E., and Bucciantini, N., 2004. Axisymmetric relativistic MHD simulations of pulsar wind nebulae in supernova remnants. On the origin of torus and jet-like features. *A&A*, 421, 1063
- [7] Del Zanna, L., Volpi, D., Amato, E., and Bucciantini, N., 2006. Simulated synchrotron emission from pulsar wind nebulae. *A&A*, 453, 621
- [8] Volpi, D., Del Zanna, L., Amato, E., and Bucciantini, N., 2008. Non-thermal emission from relativistic MHD simulations of PWNe: from synchrotron to inverse Compton. *A&A*, in press (arXiv:0804.1323)